 SID, vol.1, no.2, pp.155-169, 2005

Vibration Analysis of Damaged Circular Arches with Varying Cross-section

E. Viola [1], and F. Tornabene [2]

Abstract: In this paper, generalized differential quadrature techniques are applied to the computation of the in-plane free vibrations of thin and thick non-uniform circular arches in undamaged and damaged configurations, when various boundary conditions are considered. Structural damage is represented by one crack in different positions and with various damage levels. The crack present in a structural member can be considered as a local stiffness reduction at the fracturing section, which changes the dynamic behaviour of the structure. Much effort has been devoted to dealing with in-plane free vibration analysis of circular arches, but only a few researchers have studied cracked circular arch structures. The present analysis refers to the complete in-plane equations of motion of non-uniform circular arches, in terms of displacements and rotation. Shearing and axial deformations as well as rotary inertia are taken into account. For given geometric and boundary conditions, the presence of a crack will cause displacements and rotations of sections along the arch greater than the corresponding values resulting in an uncracked structure. In order to evaluate the effect of cracks, a cracked section is modelled as an elastic hinge with rotational constant which has to simulate the local flexibility caused by the cracked section itself. A crack will produce discontinuities in slope of the elastic curve of the arch at the fractured cross-section. It should be noted that in our investigation of the in-plane dynamic response variation of damaged arches with variable cross-section, the localized cracks will always be considered as open.

keyword: Damaged circular arches, Crack, Varying cross-section, Free vibrations, G.D.Q. method, G.D.Q.E. method.

[1] DISTART, Department of Structural Engineering, University of Bologna, Italy. E-mail: erasmo.viola@mail.ing.unibo.it, This work extends the paper presented at the 4^{th} International Conference on Fracture and Damage Mechanics (12-14 July 2005, Mallorca, Spain) [Tornabene and Viola (2005)].

[2] DISTART, Department of Structural Engineering, University of Bologna, Italy. E-mail: francesco.tornabene@mail.ing.unibo.it

1 Introduction

An innovative procedure for the solution of partial differential equations is the method of differential quadrature which was originally introduced by Bellman and Casti (1971) as a simple and highly efficient technique. This method can be used as a numerical algorithm to overcome some of the drawbacks of other methods. The mathematical fundamentals and recent developments of the generalized differential quadrature (G.D.Q.) method as well as its major applications in engineering are discussed in detail in the book by Shu (2000). As shown in the literature, see Bert and Malik (1996), the G.D.Q. is a global method which can obtain very accurate numerical results by using a considerably small number of grid points. The generalized differential quadrature method is used in this work to solve the basic governing equations of thin and thick non-uniform circular arches comprising radial and tangential as well as rotation displacements as field variables. This technique is applied to the computation of the eigenvalues of the equations of motion governing the in-plane extensional free vibration of circular arches with variable thickness and with transverse crack in a generic cross-section. It is well known that the curvilinear geometry of the arch produces a coupling between displacements and rotation in the equations of motion. However, the problem can be somewhat simplified, introducing certain assumptions on the kinematics assessment of the arch and on its inertial properties. Among the publications available in the open literature, many authors have used the simplified model with negligible rotary inertia, shearing deformation and axial extensibility which gives a singular 6^{th} order partial differential equation of motion. To improve the accuracy of natural frequency, it is suggested that the axial deformation should be taken into account. Tong, Mrad and Tabarrok (1988) have used the exact solution of inextensible thin uniform circular arches to study the in-plane free and forced vibration of circular arches with variable cross-section. As far as the application of the differential quadrature (D.Q.) method is concerned, some papers should be mentioned.

Gutierrez and Laura (1995) have used D.Q. technique in conjunction with the δ-technique [Bert, Jang and Striz (1988)] to obtain the fundamental natural frequency of continuously variable section ring type arches, while De Rosa and Franciosi (2000) have used a D.Q. method to study uniform circular arches. More recently, Liu and Wu (2001) have used the generalized differential quadrature rule to study the free vibrations of inextensible circular arches. Variable cross-section arches under different types of classical boundary conditions have been examined. As an improvement to the classical theory, Karami and Malekzadeh (2004) removed the commonly used hypothesis of the inextensibility of the central axis and included rotary inertia in their formulation. They solved the model which accounts axial deformability, governed by two coupled differential equations for the tangential and radial displacements. The present study differs from the previous ones due to the fact that here, unlike in previous cases, the complete model is employed, which takes the total of these three contributions into account and is governed by a triplet of coupled second order differential equations. The unknown rotation φ and displacements u, v have to be determined.

In this work, the in-plane linear free vibrations of non-uniform circular arches, in undamaged and damaged configurations, taking into account shearing and axial deformations and rotary inertia, are investigated. Numerous previous studies have focused on the dynamic behaviour of the arch with variable cross-section in the undamaged configuration. The purpose of this paper, therefore, is to provide a contribution in the study of the free harmonic vibration problem of circular arches with varying cross-section in damaged configuration, modelling the cracked cross-section with an elastic hinge. For each arch part between the crack and the arch end, the equations of motion have been written with no simplifying hypothesis. Once the boundary conditions and jump conditions across the damaged section have been set, the solution of the problem, in terms of natural frequencies and mode shapes, has been obtained.

It is worth noting that the G.D.Q. and the G.D.Q. element (G.D.Q.E.) methods represent computationally efficient techniques for the solution of partial differential equations because they allow us to obtain highly accurate results. These simple direct techniques can be applied in a large number of cases to circumvent the difficulties of programming complex algorithms for the computer, as well as excessive use of storage and computer time.

2 Motion Equation of the Structural Problem

Let us consider a non-uniform circular arch referred to a global system $O(X,Y,Z)$, as shown in figure 1, with different boundary conditions. Let us suppose that the system vibrates freely in the $O(X,Y)$ vertical plane, with small oscillations around a circular and unstressed configuration of equilibrium. Fig. 1 illustrates a prismatic isotropic arch having a general cross-section of area $A(s)$, moment of inertia $I(s)$, radius of curvature r, total length s_0 along the centroidal axis and full amplitude ϑ_0. The $Z=0$ plane contains the centroidal axis and is a symmetry plane for the road. A curvilinear abscissa s spans the axis line, the points of which are described by $X(s)$ and $Y(s)$ coordinates in the general system. A local reference system $o'(x(s),y(s))$ is defined according to the tangential and the normal axis at the generic abscissa of the axis line. The kinematics of the arch is thoroughly defined by assigning the tangential displacement $u(s,t)$, the normal displacement $v(s,t)$ and the rotation angle about the binormal axis $\varphi(s,t)$ of the s coordinate cross-section at a moment of time t.

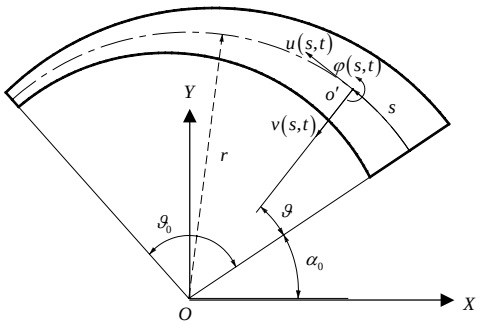

Figure 1 : Prismatic circular arch having a general cross-section

The strain displacement relations of the arch are determined using the definitions for the strain displacements in a curvilinear coordinate system. The strain displacement relations can be written as:

$$\varepsilon = \frac{\partial u(s,t)}{\partial s} - \frac{v(s,t)}{r}$$
$$\gamma = \frac{u(s,t)}{r} + \frac{\partial v(s,t)}{\partial s} + \varphi(s,t)$$
$$\chi = \frac{\partial \varphi(s,t)}{\partial s} \qquad (1)$$

in which ε and γ are the normal and shear strain components, respectively, whereas χ denotes curvature. It is worth noting that the strain-displacement relations (1) are valid when the displacements are assumed to be small.

Taking into account the effect of shear and axial deformations and rotary inertia, the equations of motion can be written as follows:

$$\begin{aligned}
&\frac{\partial N(s,t)}{\partial s}-\frac{T(s,t)}{r}=\rho A(s)\frac{\partial^2 u(s,t)}{\partial t^2}\\
&\frac{\partial T(s,t)}{\partial s}+\frac{N(s,t)}{r}=\rho A(s)\frac{\partial^2 v(s,t)}{\partial t^2}\\
&\frac{\partial M(s,t)}{\partial s}-T(s,t)=\rho I(s)\frac{\partial^2 \varphi(s,t)}{\partial t^2}
\end{aligned} \tag{2}$$

for $s \in [0, s_0]$, and $t > 0$. In the previous equations, $N(s,t)$, $T(s,t)$ and $M(s,t)$, denote the stress resultants specified as axial force, shear force and bending moment, respectively. Moreover, ρ is the mass density for unit volume.

For a homogeneous isotropic Hookean material, the internal forces can be expressed by the constitutive relations in terms of displacements:

$$\begin{aligned}
N(s,t)&=EA(s)\left(\frac{\partial u(s,t)}{\partial s}-\frac{v(s,t)}{r}\right)\\
T(s,t)&=G\Lambda(s)\left(\frac{u(s,t)}{r}+\frac{\partial v(s,t)}{\partial s}+\varphi(s,t)\right)\\
M(s,t)&=EI(s)\frac{\partial \varphi(s,t)}{\partial s}
\end{aligned} \tag{3}$$

in which E and G are the well known Young's and shear modules and $\Lambda = A/k_0$ where k_0 denotes the shear correction factor.

Substituting relations (3) in (2), the equations of motion can be written in terms of displacement components as:

$$\begin{aligned}
&\frac{\partial}{\partial s}\left(EA(s)\left(\frac{\partial u(s,t)}{\partial s}-\frac{v(s,t)}{r}\right)\right)\\
&\quad-\frac{G\Lambda(s)}{r}\left(\frac{u(s,t)}{r}+\frac{\partial v(s,t)}{\partial s}+\varphi(s,t)\right)\\
&\quad=\rho A(s)\frac{\partial^2 u(s,t)}{\partial t^2}\\
&\frac{\partial}{\partial s}\left(G\Lambda(s)\left(\frac{u(s,t)}{r}+\frac{\partial v(s,t)}{\partial s}+\varphi(s,t)\right)\right)\\
&\quad+\frac{EA(s)}{r}\left(\frac{\partial u(s,t)}{\partial s}-\frac{v(s,t)}{r}\right)\\
&\quad=\rho A(s)\frac{\partial^2 v(s,t)}{\partial t^2}\\
&\frac{\partial}{\partial s}\left(EI(s)\frac{\partial \varphi(s,t)}{\partial s}\right)\\
&\quad-G\Lambda(s)\left(\frac{u(s,t)}{r}+\frac{\partial v(s,t)}{\partial s}+\varphi(s,t)\right)\\
&\quad=\rho I(s)\frac{\partial^2 \varphi(s,t)}{\partial t^2}
\end{aligned} \tag{4}$$

In equations (4), it is noted that the effects of axial deformation, shear deformation and rotary inertia are considered. The coupled system of second order differential equations (4), which represents the equilibrium equations in terms of displacements $u = u(s,t)$, $v = v(s,t)$ and $\varphi = \varphi(s,t)$, contains all the three aspects of the problem of elastic equilibrium, namely equilibrium equations, strain-displacement and constitutive relations.

Then, assuming non-uniform circular cross-section and constant material properties through the arch, the equations (4) can be rewritten as:

$$\begin{aligned}
&EA\frac{\partial^2 u}{\partial s^2}+E\frac{dA}{ds}\frac{\partial u}{\partial s}-\frac{G\Lambda}{r^2}u-\left(\frac{EA}{r}+\frac{G\Lambda}{r}\right)\frac{\partial v}{\partial s}\\
&-E\frac{dA}{ds}\frac{v}{r}-\frac{G\Lambda}{r}\varphi=\rho A\frac{\partial^2 u}{\partial t^2}\\
&G\Lambda\frac{\partial^2 v}{\partial s^2}+\frac{G}{k_0}\frac{dA}{ds}\frac{\partial v}{\partial s}-\frac{EA}{r^2}v+\left(\frac{EA}{r}+\frac{G\Lambda}{r}\right)\frac{\partial u}{\partial s}\\
&+\frac{G}{k_0}\frac{dA}{ds}\frac{u}{r}+G\Lambda\frac{\partial \varphi}{\partial s}+\frac{G}{k_0}\frac{dA}{ds}\varphi=\rho A\frac{\partial^2 v}{\partial t^2}\\
&EI\frac{\partial^2 \varphi}{\partial s^2}+E\frac{dI}{ds}\frac{\partial \varphi}{\partial s}-G\Lambda\varphi-G\Lambda\frac{u}{r}-G\Lambda\frac{\partial v}{\partial s}\\
&=\rho I\frac{\partial^2 \varphi}{\partial t^2}
\end{aligned} \tag{5}$$

Equations (5) are the governing equations for the in-plane free vibrations of arches with varying cross-section.

Using the separation of variables, it is possible to seek solutions that are harmonic in time and which have a frequency of ω; then, the axial and radial displacements and

the rotation angle can be written as follows:

$$\begin{aligned} u(s,t) &= U(s)e^{i\omega t} \\ v(s,t) &= V(s)e^{i\omega t} \\ \varphi(s,t) &= \Phi(s)e^{i\omega t} \end{aligned} \tag{6}$$

where the vibration spatial amplitude values $(U(s),V(s),\Phi(s))$ fulfil the fundamental differential system:

$$\begin{aligned} &EA\frac{d^2U}{ds^2}+E\frac{dA}{ds}\frac{dU}{ds}-\frac{G\Lambda}{r^2}U-\left(\frac{EA}{r}+\frac{G\Lambda}{r}\right)\frac{dV}{ds} \\ &-E\frac{dA}{ds}\frac{V}{r}-\frac{G\Lambda}{r}\Phi=-\omega^2\rho AU \\ &G\Lambda\frac{d^2V}{ds^2}+\frac{G}{k_0}\frac{dA}{ds}\frac{dV}{ds}-\frac{EA}{r^2}V+\left(\frac{EA}{r}+\frac{G\Lambda}{r}\right)\frac{dU}{ds} \\ &+\frac{G}{k_0}\frac{dA}{ds}\frac{U}{r}+G\Lambda\frac{d\Phi}{ds}+\frac{G}{k_0}\frac{dA}{ds}\Phi=-\omega^2\rho AV \\ &EI\frac{d^2\Phi}{ds^2}+E\frac{dI}{ds}\frac{d\Phi}{ds}-G\Lambda\Phi-G\Lambda\frac{U}{r}-G\Lambda\frac{dV}{ds} \\ &=-\omega^2\rho I\Phi \end{aligned} \tag{7}$$

In this paper, three kinds of boundary conditions are considered at each end of the arch, namely the fully clamped edge boundary condition (C), the simply supported edge boundary condition (S) and the free edge boundary condition (F). The equations describing the boundary conditions can be written as follows:

1. Clamped edge boundary condition (C):

$$u(s,t)=0,\ v(s,t)=0,\ \varphi(s,t)=0 \quad at \quad s=0 \quad or \quad s=s_0 \tag{8}$$

2. Simply supported edge boundary condition (S):

$$u(s,t)=0,\ v(s,t)=0,\ M(s,t)=0 \quad at \quad s=0 \quad or \quad s=s_0 \tag{9}$$

3. Free edge boundary condition (F):

$$N(s,t)=0,\ T(s,t)=0,\ M(s,t)=0 \quad at \quad s=0 \quad or \quad s=s_0 \tag{10}$$

3 G.D.Q.E. Technique

The G.D.Q. method will be used to discretize the derivatives in the governing equations and the boundary conditions. The G.D.Q. approach was developed by Shu and Richards (1992) to improve the D.Q. technique for the computation of weighting coefficients. The essence of the differential quadrature method is that, the partial or total derivate of a smooth function with respect to a variable is approximated by a weighted sum of function values at all discrete points in that direction. The weighting coefficients are not related to any special problem and only depend on the grid points and the derivate order. In this methodology, an arbitrary grid distribution can be chosen without any limitation.

Thus, the n^{th} order derivative of function $f(s)$ with respect to s at a grid points s_i, can be approximated by the G.D.Q. approach:

$$\left.\frac{\partial^n f(s)}{\partial s^n}\right|_{s=s_i}=\sum_{j=1}^{N}\varsigma_{ij}^{(n)}f(s_j), \quad i=1,2,.....,N \tag{11}$$

where $\varsigma_{ij}^{(n)}$ are the weighting coefficients of the n^{th} order derivative at the i^{th} sampling points along the domain. N is the total number of the sampling points of the grid distribution and $f(s_j)$ are the function values at grid points.

The weighting coefficients can be determined by the chosen interpolation rule. For the cases treated in the present paper, Lagrange polynomial functions have been adopted.

The Lagrange interpolated polynomials can be defined by the formula:

$$p_j(s)=\frac{L(s)}{(s-s_j)L^{(1)}(s_j)}, \quad j=1,....,N \tag{12}$$

where:

$$L(s)=\prod_{i=1}^{N}(s-s_i), \quad L^{(1)}(s_j)=\prod_{i=1,i\neq j}^{N}(s_j-s_i) \tag{13}$$

With this choice, some simple recursive formulas are available for finding weighting coefficients [Shu (1991)]. For the first order derivative, we have:

$$\varsigma_{ij}^{(1)}=\frac{L^{(1)}(s_i)}{(s_i-s_j)L^{(1)}(s_j)}, \ i,j=1,2,.....,N, \quad i\neq j \tag{14}$$

For higher order derivatives, one gets iteratively:

$$\varsigma_{ij}^{(n)} = n\left(\varsigma_{ii}^{(n-1)}\varsigma_{ij}^{(1)} - \frac{\varsigma_{ij}^{(n-1)}}{s_i - s_j}\right),$$
$$i \neq j,\ n = 2,3,.....,N-1,\ i,j = 1,2,.....,N \quad (15)$$

$$\sum_{j=1}^{N}\varsigma_{ij}^{(n)} = 0 \ \Rightarrow\ \varsigma_{ii}^{(n)} = -\sum_{j=1,j\neq i}^{N}\varsigma_{ij}^{(n)},$$
$$n = 1,2,3,.....,N-1,\quad i,j = 1,2,.....,N \quad (16)$$

Civan and Sliepcevich (1985) introduced domain decomposition technique with D.Q. method for the first time. The G.D.Q. method may be employed as an efficient numerical tool for solving the domain problems which have every form of discontinuity in geometry, material or loading and boundary conditions in the form of sub-domain elements to be called G.D.Q.E. [Chen (2000)]. As with the finite element method (FEM), in the G.D.Q.E. method the domain of a problem is first separated into a certain number of sub-domains or elements. Then, the G.D.Q. discretization is carry out on each element. The governing differential or partial differential equations defined on each element, the transition conditions on inter-element boundaries and the boundary conditions on the domain boundary are in computable form after G.D.Q. discretization. Assembling all the discrete fundamental equations, the overall algebraic system can be obtained and used to solve the problem. Fig. 2 shows a generic arch with different constant thicknesses. For such problems, the vector of boundary degree of freedom should be modified to include the displacements at the common section of each of the two adjacent sub-domains.

The governing equations of each sub-domain are similar to those of a single domain obtained before. In addition to the external boundary conditions, the kinematical and physical compatibility should be satisfied at the common section s^* of the two adjacent sub-domains.

The kinematical compatibility conditions include the continuity of axial and radial displacements as well as rotation. The physical compatibility conditions can only be the three continuous conditions for the bending moment, shear force and axial force at the domain decomposition point.

The kinematical compatibility at the generic abscissa s^*,

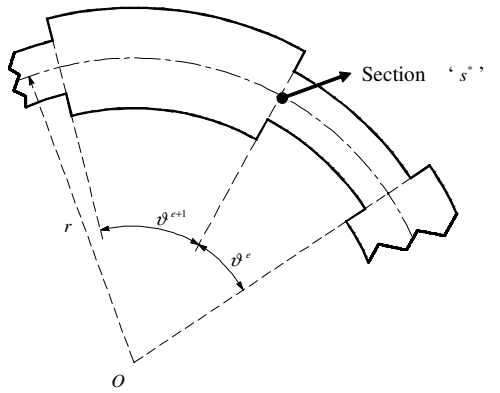

Figure 2 : Two adjacent sub-domains 'e+1' and 'e' at the common section 's^*'

where the discontinuity occurs, may be stated as:

$$u^{e+1}(s^*,t) - u^e(s^*,t) = 0$$
$$v^{e+1}(s^*,t) - v^e(s^*,t) = 0$$
$$\varphi^{e+1}(s^*,t) - \varphi^e(s^*,t) = 0 \quad (17)$$

and the physical compatibility conditions require that:

$$N^{(e+1)}(s^*,t) - N^{(e)}(s^*,t) = 0$$
$$T^{(e+1)}(s^*,t) - T^{(1)}(s^*,t) = 0$$
$$M^{(e+1)}(s^*,t) - M^{(e)}(s^*,t) = 0 \quad (18)$$

Usually, as in this paper, the same number of sampling points $N^e = N$ for each sub-domain 'e' is used to simplify the computational program.

With Lagrange interpolating polynomials, the Chebyshev-Gauss-Lobatto sampling point rule proves efficient for numerical reasons [Shu, Chen, Xue and Du (2001)], so that for such a collocation the approximation error of dependent variable decreases as the number of nodes increases. For the numerical computations presented in this paper, the coordinates of grid points are chosen as:

$$s_i = \frac{1-\cos\left(\frac{i-1}{N^e-1}\right)\pi}{2}s^e, \quad i = 1,....,N^e \quad (19)$$

where s^e is the length of each arch element generated by every form of discontinuity in geometry, material or loading, while N^e is the total number of sampling points used to discretize each arch element.

4 Crack Modelling

In the present study, the transverse crack has been considered as open. A damaged arch is now considered, in which the damage is localized at a generic section labelled by the angle $\vartheta_{cr} \in]0, \vartheta_0[$. A cracked arch can be viewed as a continuum with a local stiffness reduction at the fracturing section. A fracture at a particular cross-section produces a discontinuity in slope of the elastic curve of the arch at the cross-section itself. In other words, a crack oriented normally to the axis of the arch can be assumed to produce only a local change in slope without altering the overall mode shape substantially from that of the corresponding uncracked arch. The notched section is modelled as an elastic hinge with a rotational constant K_φ chosen to simulate the notch effects, as first proposed by Chondras and Dimarogonas (1980).

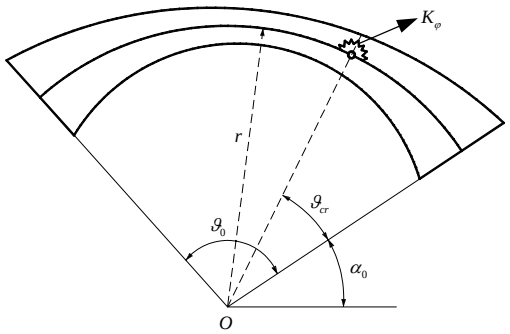

Figure 3 : Notched section modelled as an elastic hinge

If the crack always remains open during the vibration of the arch, it can be modelled as a massless rotational elastic spring at the damaged cross-section [Viola, Federici and Nobile (2001), Viola, Nobile and Federici (2002)]. The stiffness K_φ of the spring can be related in a precise way to the geometry of damage, as suggested, for example, by Rizos, Aspragathos and Dimarogonas (1990). For the vibration analysis the arch is split into two unnotched arch elements joined together at the fracturing section by a rotational spring.

The conditions at the fracturing section $s = s_{cr}$ can be written for the kinematical compatibility as:

$$\begin{aligned} &u^{(e+1)}(s_{cr},t) - u^{(e)}(s_{cr},t) = 0 \\ &v^{(e+1)}(s_{cr},t) - v^{(e)}(s_{cr},t) = 0 \\ &K_\varphi \left(\varphi^{(e+1)}(s_{cr},t) - \varphi^{(e)}(s_{cr},t) \right) = M^{(e)}(s_{cr},t) \end{aligned} \tag{20}$$

The nodal equilibrium conditions at $s = s_{cr}$ are:

$$\begin{aligned} &N^{(e+1)}(s_{cr},t) - N^{(e)}(s_{cr},t) = 0 \\ &T^{(e+1)}(s_{cr},t) - T^{(e)}(s_{cr},t) = 0 \\ &M^{(e+1)}(s_{cr},t) - M^{(e)}(s_{cr},t) = 0 \end{aligned} \tag{21}$$

The undamaged arch corresponds to $K_\varphi \to \infty$, or, equivalently, to $\varphi^{(e+1)}(s_{cr},t) - \varphi^{(e)}(s_{cr},t) = 0$. In the following section the case of an arch with varying cross-section in undamaged and damaged configurations, having constant elastic properties in each element, will be investigated.

5 Numerical Implementation

The numerical operations illustrated above enable one to write the equations of motion in discrete form, transforming every space derivative into a weighted sum of node values of dependent variables applying the G.D.Q. procedure. Each triplet of approximated equations is valid in a single sampling point belonging to one of the arch segments. For the generic arch element 'e' and its interior sampling points, $i = 2, 3, ..., N^e - 1$, the governing equations can be discretized as follows:

$$\begin{aligned} &E^e A_i^e \sum_{j=1}^{N^e} \varsigma_{ij}^{(2)e} U_j^e + E^e \sum_{j=1}^{N^e} \varsigma_{ij}^{(1)e} A_j^e \sum_{j=1}^{N^e} \varsigma_{ij}^{(1)e} U_j^e - \frac{G^e \Lambda_i^e}{r^2} U_i^e \\ &- \left(\frac{E^e A_i^e}{r} + \frac{G^e \Lambda_i^e}{r} \right) \sum_{j=1}^{N^e} \varsigma_{ij}^{(1)e} V_j^e - \frac{E^e}{r} V_i^e \sum_{j=1}^{N^e} \varsigma_{ij}^{(1)e} A_j^e \\ &- \frac{G^e \Lambda_i^e}{r} \Phi_i^e = -\omega^2 \rho^e A_i^e U_i^e \\ &G^e \Lambda_i^e \sum_{j=1}^{N^e} \varsigma_{ij}^{(2)e} V_j^e + \frac{G^e}{k_0} \sum_{j=1}^{N^e} \varsigma_{ij}^{(1)e} A_j^e \sum_{j=1}^{N^e} \varsigma_{ij}^{(1)e} V_j^e - \frac{E^e A_i^e}{r^2} V_i^e \\ &+ \left(\frac{E^e A_i^e}{r} + \frac{G^e \Lambda_i^e}{r} \right) \sum_{j=1}^{N^e} \varsigma_{ij}^{(1)e} U_j^e + \frac{G^e}{k_0 r} U_i^e \sum_{j=1}^{N^e} \varsigma_{ij}^{(1)e} A_j^e \\ &+ G^e \Lambda_i^e \sum_{j=1}^{N^e} \varsigma_{ij}^{(1)e} \Phi_j^e + \frac{G^e}{k_0} \Phi_i^e \sum_{j=1}^{N^e} \varsigma_{ij}^{(1)e} A_j^e = -\omega^2 \rho^e A_i^e V_i^e \\ &E^e I_i^e \sum_{j=1}^{N^e} \varsigma_{ij}^{(2)e} \Phi_j^e + E^e \sum_{j=1}^{N^e} \varsigma_{ij}^{(1)e} I_j^e \sum_{j=1}^{N^e} \varsigma_{ij}^{(1)e} \Phi_j^e - G^e \Lambda_i^e \Phi_i^e \\ &- \frac{G^e \Lambda_i^e}{r} U_i^e - G^e \Lambda_i^e \sum_{j=1}^{N^e} \varsigma_{ij}^{(1)e} V_j^e = -\omega^2 \rho^e I_i^e \Phi_i^e \end{aligned} \tag{22}$$

Applying the G.D.Q. methodology, the discretized forms of the boundary conditions are given as follows:

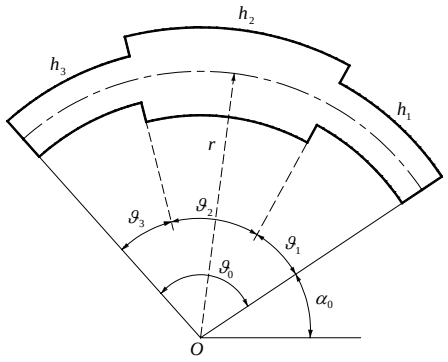

Figure 4 : Stepped arch with two section discontinuities

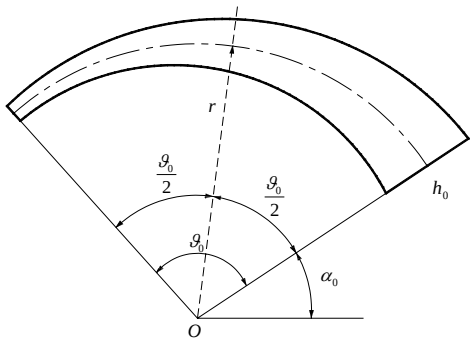

Figure 5 : Tapered arch with a linear unsymmetric height variation

1. Clamped edge boundary condition (C):

$$U_i^e = 0,\ V_i^e = 0,\ \Phi_i^e = 0 \qquad for\ i = 1\ or\ i = N^e \tag{23}$$

2. Simply supported edge boundary condition (S):

$$U_i^e = 0,\ V_i^e = 0,\ \sum_{j=1}^{N^e} \varsigma_{ij}^{(1)e} \Phi_j^e = 0 \qquad for\ i = 1\ or\ i = N^e \tag{24}$$

3. Free edge boundary condition (F):

$$\sum_{j=1}^{N^e} \varsigma_{ij}^{(1)e} U_j^e - \frac{V_i^e}{r} = 0,\ \sum_{j=1}^{N^e} \varsigma_{ij}^{(1)e} V_j^e + \frac{U_i^e}{r} + \Phi_i^e = 0,$$
$$\sum_{j=1}^{N^e} \varsigma_{ij}^{(1)e} \Phi_j^e = 0 \quad \text{for } i = 1\ or\ i = N^e \tag{25}$$

where N^e is the number of sampling points for the arch element 'e'.

It should be noted that in correspondence of each discontinuity regarding the properties of the arch, the jump conditions must be imposed by means of the G.D.Q. method:

$$\begin{aligned}
&U_1^{e+1} = U_{N^e}^e \\
&\quad \sum_{j=1}^{N^{e+1}} \varsigma_{1j}^{(1)e+1} U_j^{e+1} - \frac{V_i^{e+1}}{r} = \sum_{j=1}^{N^e} \varsigma_{N^e j}^{(1)e} U_j^e - \frac{V_i^e}{r} \\
&V_1^{e+1} = V_{N^e}^e \\
&\quad \sum_{j=1}^{N^{e+1}} \varsigma_{1j}^{(1)e+1} V_j^{e+1} + \frac{U_1^{e+1}}{r} + \Phi_1^{e+1} \\
&\quad = \sum_{j=1}^{N^e} \varsigma_{N^e j}^{(1)e} V_j^e + \frac{U_{N^e}^e}{r} + \Phi_{N^e}^e \\
&\Phi_1^{e+1} = \Phi_{N^e}^e \\
&\quad \sum_{j=1}^{N^{e+1}} \varsigma_{1j}^{(1)e+1} \Phi_j^{e+1} = \sum_{j=1}^{N^e} \varsigma_{N^e j}^{(1)e} \Phi_j^e
\end{aligned} \tag{26}$$

In presence of crack, the jump conditions can be written in discrete form as:

$$\begin{aligned}
&U_1^{e+1} = U_{N^e}^e \\
&\quad \sum_{j=1}^{N^{e+1}} \varsigma_{1j}^{(1)e+1} U_j^{e+1} - \frac{V_i^{e+1}}{r} = \sum_{j=1}^{N^e} \varsigma_{N^e j}^{(1)e} U_j^e - \frac{V_i^e}{r} \\
&V_1^{e+1} = V_{N^e}^e \\
&\quad \sum_{j=1}^{N^{e+1}} \varsigma_{1j}^{(1)e+1} V_j^{e+1} + \frac{U_1^{e+1}}{r} + \Phi_1^{e+1} \\
&\quad = \sum_{j=1}^{N^e} \varsigma_{N^e j}^{(1)e} V_j^e + \frac{U_{N^e}^e}{r} + \Phi_{N^e}^e \\
&K_\varphi \left(\Phi_1^{e+1} - \Phi_{N^e}^e \right) = E^e I_{N^e}^e \sum_{j=1}^{N^e} \varsigma_{N^e j}^{(1)e} \Phi_j^e, \\
&\quad \sum_{j=1}^{N^{e+1}} \varsigma_{1j}^{(1)e+1} \Phi_j^{e+1} = \sum_{j=1}^{N^e} \varsigma_{N^e j}^{(1)e} \Phi_j^e
\end{aligned} \tag{27}$$

Applying the differential quadrature procedure, the whole system of differential equations can be discretized and the global assembling leads to the following set of linear algebraic equations:

$$\begin{bmatrix} \mathbf{K}_{bb} & \mathbf{K}_{bd} \\ \mathbf{K}_{db} & \mathbf{K}_{dd} \end{bmatrix} \begin{bmatrix} \delta_b \\ \delta_d \end{bmatrix} = \omega^2 \begin{bmatrix} \mathbf{0} & \mathbf{0} \\ \mathbf{0} & \mathbf{M}_{dd} \end{bmatrix} \begin{bmatrix} \delta_b \\ \delta_d \end{bmatrix} \tag{28}$$

In the above matrices and vector, the partitioning is set forth by subscripts b and d, referring to the system degrees of freedom and standing for *boundary* and *domain*,

respectively. In order to make the computation more efficient, kinematic condensation of non-domain degrees of freedom is performed:

$$\left(\mathbf{K}_{dd}-\mathbf{K}_{db}\left(\mathbf{K}_{bb}\right)^{-1}\mathbf{K}_{bd}\right)\delta_d=\omega^2\mathbf{M}_{dd}\delta_d \tag{29}$$

The natural frequencies of the structure considered can be determined by making the following determinant equal zero:

$$\left|\left(\mathbf{K}_{dd}-\mathbf{K}_{db}\left(\mathbf{K}_{bb}\right)^{-1}\mathbf{K}_{bd}\right)-\omega^2\mathbf{M}_{dd}\right|=0 \tag{30}$$

6 Applications and Results

Based on the above derivations, in the present paragraph some results and considerations about the free vibration problem of non-uniform circular arches with different boundary conditions in damaged and undamaged configurations are presented. The analysis has been carried out by means of numerical procedures illustrated above. Various typologies of rectangular cross-section arches, with constant width b, are considered: the arch with uniform cross-section, the stepped arch and the tapered arch. In particular, for the tapered arch, two kinds of cross-sectional height variation are examinated.

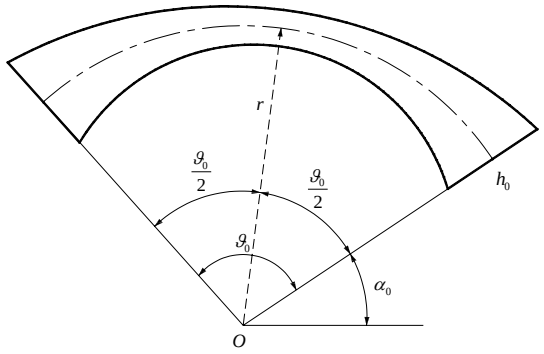

Figure 6 : Tapered arch with a quadratic symmetric height variation

The cross-sectional height for these cases varies as:

Linear unsymmetric variation

$$1)\ h(s)=h_0\left(1-\eta\frac{s}{s_0}\right) \qquad 0\le\eta<1 \tag{31}$$

Quadratic symmetric variation

$$2)\ h(s)=\frac{h_0}{s_0^2}\left(s_0^2-2s_0s+2s^2\right) \tag{32}$$

where s_0 is the total length of the arch, h_0 is the height at the right end of the arch and η is the taper parameter. The kinds of variation of arch height are shown in Figs. 5 and 6. The Chebyshev-Gauss-Lobatto grid is employed in all examples in this work.

The main purpose of this study is to emphasize how the modal parameters vary with the damage level and cracking location. In the following, numerical results related to different non-uniform circular arches - the mechanical characteristics of which are listed in Tab. 1 - are presented. Different damage locations ϑ_{cr} and two damage levels have been considered. For the two damage levels, the stiffnesses of the rotational spring are (1) $K_\varphi=10EI$ and (2) $K_\varphi=EI$, respectively.

Table 1 : Physical parameters used in the analysis of free vibrations of the arches being considered.

Parameter	Value
Density of mass ρ	7860 kg / m^3
Young's modulus E	$2.1\cdot10^{11}$Pa
Poisson coefficient ν	0.3
Shear factor k_0	1.2

In order to verify the accuracy, Tab. 2 shows the first eight eigenfrequencies corresponding to the clamped-clamped uniform arch. The exact solution is compared to the G.D.Q.E. solution for the damaged arch with a rotational elastic hinge. It is evident how the G.D.Q.E. technique produces coincident results, when compared to the analytical ones, using only a few sampling points along the two sub-domains. Some new results for non-uniform arches with different boundary conditions, α_0 opening angle, ϑ_0 full amplitude and damage locations ϑ_{cr} are presented in Tabs. 3-6. Tab. 3 shows the first eigenfrequencies of clamped-clamped and hinged-hinged two stepped circular arches with two different locations and severities of the damage.

The second location of the damage is in the same section where the discontinuity of the cross-sectional height occurs. In this case, the stiffness of the rotational is related to the shortest thickness of the stepped arch. As shown on Tab. 3, the frequencies decrease when the damage level increases. Tabs. 4 and 5 show other typologies of variable section arch with different end conditions. The first frequencies for a linearly varying height of the arch cross-section are listed for different damage positions.

Table 2 : Frequencies for a uniform clamped-clamped circular arch with centroidal axis radius $r = 1\,m$, width $b = 0.06\,m$ and constant thickness $h_0 = 0.08m$ in undamaged and damaged configurations. Stiffnesses of the rotational spring are respectively: (1) $K_\varphi = 10EI$, (2) $K_\varphi = EI$. The material properties are reported in Table 1.

Mode	Undamaged		Damaged (1)		Damaged (2)	
[Hz]	Exact	G.D.Q.	Exact	G.D.Q.	Exact	G.D.Q.
Circular arch with constant thickness: $\vartheta_0 = 100^\circ$, $\alpha_0 = 40^\circ$						
Angular coordinate of the damage: $\vartheta_{cr} = 60^\circ$						
1	328.2	328.18	321.4	321.40	295.1	295.06
2	546.6	546.57	540.6	540.58	520.9	520.91
3	854.1	854.14	852.0	851.97	838.8	838.76
4	1078.5	1078.46	1037.1	1037.12	939.8	939.84
5	1642.0	1642.02	1636.0	1635.97	1612.2	1612.22
6	1646.3	1646.32	1642.9	1642.86	1642.6	1642.62
7	2240.2	2240.22	2177.8	2177.81	2047.9	2047.89
8	2813.9	2813.93	2777.2	2777.16	2716.3	2716.28
Angular coordinate of the damage: $\vartheta_{cr} = 80^\circ$						
1	328.2	328.18	323.3	323.32	302.7	302.67
2	546.6	546.57	533.7	533.67	493.3	493.29
3	854.1	854.14	842.3	842.33	806.9	806.90
4	1078.5	1078.46	1055.4	1055.42	1010.6	1010.59
5	1642.0	1642.02	1626.2	1626.24	1588.5	1588.45
6	1646.3	1646.32	1644.4	1644.43	1644.3	1644.26
7	2240.2	2240.22	2236.7	2236.73	2225.9	2225.92
8	2813.9	2813.93	2751.4	2751.43	2592.6	2592.64
Angular coordinate of the damage: $\vartheta_{cr} = 90^\circ$						
1	328.2	328.18	326.6	326.56	322.0	321.99
2	546.6	546.57	544.6	544.61	539.2	539.19
3	854.1	854.14	853.4	853.35	850.8	850.78
4	1078.5	1078.46	1068.6	1068.61	1039.1	1039.13
5	1642.0	1642.02	1610.0	1609.96	1520.4	1520.37
6	1646.3	1646.32	1646.2	1646.20	1646.2	1646.19
7	2240.2	2240.22	2182.6	2182.59	2063.8	2063.78
8	2813.9	2813.93	2755.8	2755.82	2664.9	2664.87

Finally, Tab. 6 shows the frequencies of the arch with quadratic varying cross-section for different damage locations and boundary conditions. The frequencies appear to be dependent on both crack position and damage severity, as well as on the boundary conditions, as one can infer from Tabs. 2-6. As expected, the frequency decreases with the damage severity, i.e. as the elastic stiffness of rotational spring decreases. For a fixed value of the elastic stiffness of rotational spring, the frequency variations depend on the crack position along the arch.

The convergence and the stability of the first five fundamental natural frequencies for non-uniform damaged circular arch with different boundary conditions are shown in Figs. 7 and 8. As reported, well converged results for the first five frequencies can be obtained with $N = 17$.

Comparing the results, one could conclude that in these cases using $N = 17$ yields very accurate values. However, it is to be noted that, when passing from undamaged configurations to damaged ones, for the first five modes more grid points are needed, to compute the correct eigenparameters.

It is shown that the accuracy of the numerical solution is steady with increasing N and does not decrease due to numerical instabilities even if N becomes too large.

Table 3 : Frequencies for two stepped arches with centroidal axis radius $r = 1\,m$, width $b = 0.1\,m$ and different constant thicknesses $h_1 = 0.08\,m$ and $h_2 = 0.06\,m$ in undamaged and damaged configurations. Stiffnesses of the rotational spring are respectively: (1) $K_\varphi = 10EI$, (2) $K_\varphi = EI$. The material properties are reported in Table 1.

		Mode sequences [Hz]				
		1	2	3	4	5
Stepped circular arch: $\vartheta_0 = 100^\circ$, $\alpha_0 = 40^\circ$, $\vartheta_1 = 30^\circ$, $\vartheta_2 = 70^\circ$						
Angular coordinate of the damage: $\vartheta_{cr} = 60^\circ$						
C-C	Undamaged	272.79	496.95	794.69	915.99	1377.42
	Damaged (1)	268.58	486.37	793.49	883.24	1377.20
	Damaged (2)	251.92	452.59	779.95	817.42	1376.53
Angular coordinate of the damage: $\vartheta_{cr} = 30^\circ$						
C-C	Undamaged	272.79	496.95	794.69	915.99	1377.42
	Damaged (1)	260.71	482.86	781.57	915.61	1343.09
	Damaged (2)	225.02	453.78	756.31	914.97	1266.29
Angular coordinate of the damage: $\vartheta_{cr} = 60^\circ$						
S-S	Undamaged	164.82	399.17	734.42	782.46	1164.71
	Damaged (1)	162.92	388.34	712.10	779.86	1162.64
	Damaged (2)	154.88	350.52	653.63	777.46	1156.44
Angular coordinate of the damage: $\vartheta_{cr} = 30^\circ$						
S-S	Undamaged	164.82	399.18	734.43	782.47	1164.71
	Damaged (1)	153.69	389.60	734.00	774.78	1118.67
	Damaged (2)	118.91	368.20	731.55	755.35	1027.11

Table 4 : Frequencies for the linear tapered arches with centroidal axis radius $r = 1\,m$, width $b = 0.1\,m$ and cross-sectional height variation (1) with $h_0 = 0.08\,m$ in undamaged and damaged configurations. Stiffnesses of the rotational spring are respectively: (1) $K_\varphi = 10EI$, (2) $K_\varphi = EI$. The material properties are reported in Table 1.

		Mode sequences [Hz]				
		1	2	3	4	5
Linear tapered circular arch: $\vartheta_0 = 140^\circ$, $\alpha_0 = 20^\circ$, $\eta = 0.75$						
Angular coordinate of the damage: $\vartheta_{cr} = 120^\circ$						
C-C	Undamaged	87.74	177.65	324.25	475.29	689.83
	Damaged (1)	85.76	172.27	318.032	474.78	686.10
	Damaged (2)	78.06	157.27	303.74	473.56	670.37
Angular coordinate of the damage: $\vartheta_{cr} = 60^\circ$						
C-C	Undamaged	87.74	177.65	324.25	475.29	689.83
	Damaged (1)	85.25	177.41	316.89	466.03	689.70
	Damaged (2)	74.25	176.43	288.68	441.71	689.08
Angular coordinate of the damage: $\vartheta_{cr} = 120^\circ$						
S-S	Undamaged	49.38	133.27	258.44	407.31	599.40
	Damaged (1)	47.42	129.51	256.12	407.09	588.96
	Damaged (2)	39.37	118.63	249.99	406.39	552.21
Angular coordinate of the damage: $\vartheta_{cr} = 60^\circ$						
S-S	Undamaged	49.38	133.27	258.44	407.31	599.40
	Damaged (1)	47.92	133.27	250.62	401.87	596.99
	Damaged (2)	40.85	133.08	221.01	386.44	588.03

Table 5 : Frequencies for the quadratic tapered arch with centroidal axis radius $r = 1\,m$, width $b = 0.1\,m$ and cross-sectional height variation (2) with $h_0 = 0.08\,m$ in undamaged and damaged configurations. Stiffnesses of the rotational spring are respectively: (1) $K_\varphi = 10EI$, (2) $K_\varphi = EI$. The material properties are reported in Table 1.

		Mode sequences [Hz]				
		1	2	3	4	5
Linear tapered circular arch: $\vartheta_0 = 70°$, $\alpha_0 = 0°$, $\eta = 0.8$						
Angular coordinate of the damage: $\vartheta_{cr} = 30°$						
C-F	Undamaged	69.80	229.04	543.78	993.71	1492.31
	Damaged (1)	66.52	224.89	518.64	993.44	1448.58
	Damaged (2)	48.92	208.08	449.27	992.63	1327.23
Angular coordinate of the damage: $\vartheta_{cr} = 50°$						
C-F	Undamaged	69.80	229.04	543.78	993.71	1492.31
	Damaged (1)	68.99	213.29	516.54	992.82	1446.19
	Damaged (2)	61.96	150.64	456.50	990.43	1316.92
Angular coordinate of the damage: $\vartheta_{cr} = 30°$						
C-S	Undamaged	409.27	631.05	954.34	1377.57	2065.16
	Damaged (1)	388.15	627.80	944.67	1347.97	1984.56
	Damaged (2)	319.05	620.07	917.01	1273.65	1839.79
Angular coordinate of the damage: $\vartheta_{cr} = 60°$						
C-S	Undamaged	409.27	631.05	954.34	1377.57	2065.16
	Damaged (1)	383.33	629.39	923.11	1371.81	2059.98
	Damaged (2)	324.83	626.41	872.71	1362.94	2042.82

Table 6 : Frequencies for the linear tapered arch with centroidal axis radius $r = 1\,m$, width $b = 0.1\,m$ and cross-sectional height variation (1) with $h_0 = 0.1\,m$ in undamaged and damaged configurations. Stiffnesses of the rotational spring are respectively: (1) $K_\varphi = 10EI$, (2) $K_\varphi = EI$. The material properties are reported in Table 1.

		Mode sequences [Hz]				
		1	2	3	4	5
Quadratic tapered circular arch: $\vartheta_0 = 120°$, $\alpha_0 = 30°$						
Angular coordinate of the damage: $\vartheta_{cr} = 40°$						
C-C	Undamaged	170.63	309.73	538.37	701.81	883.34
	Damaged (1)	165.10	306.64	534.48	686.22	867.63
	Damaged (2)	145.65	297.71	519.52	643.87	837.78
Angular coordinate of the damage: $\vartheta_{cr} = 70°$						
C-C	Undamaged	170.63	309.73	538.37	701.81	883.34
	Damaged (1)	167.17	306.76	517.99	701.81	882.79
	Damaged (2)	154.70	296.79	468.08	701.81	880.71
Angular coordinate of the damage: $\vartheta_{cr} = 40°$						
S-S	Undamaged	82.16	217.90	408.36	632.32	814.29
	Damaged (1)	78.74	217.16	400.50	610.65	811.36
	Damaged (2)	65.58	214.54	372.63	561.34	805.53
Angular coordinate of the damage: $\vartheta_{cr} = 70°$						
S-S	Undamaged	82.16	217.90	408.36	632.32	814.29
	Damaged (1)	80.74	214.71	393.63	632.17	814.28
	Damaged (2)	75.12	202.87	355.12	631.76	813.59

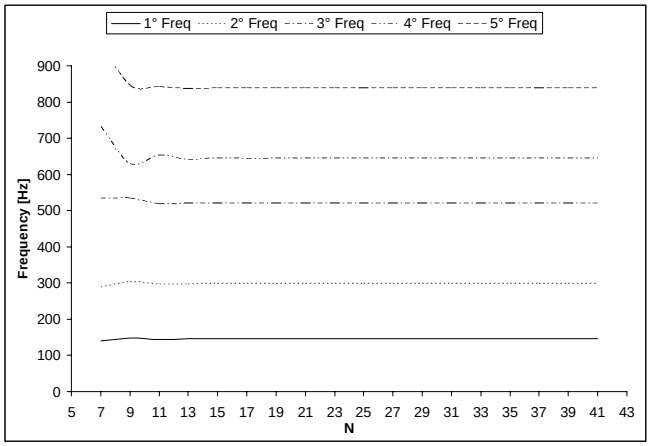

Figure 7 : Convergence characteristics of the first five frequencies for the clamped-clamped tapered arch with centroidal axis radius $r = 1\,m$, width $b = 0.1\,m$, full amplitude $\vartheta_0 = 120^\circ$ and quadratic cross-sectional height variation with $h_0 = 0.08\,m$, $\alpha_0 = 30^\circ$ in damaged configuration. The stiffness of the rotational spring is $K_\varphi = EI$. Angular coordinate of the cracked cross-section: $\vartheta_{cr} = 40^\circ$. The material properties are reported in Table 1.

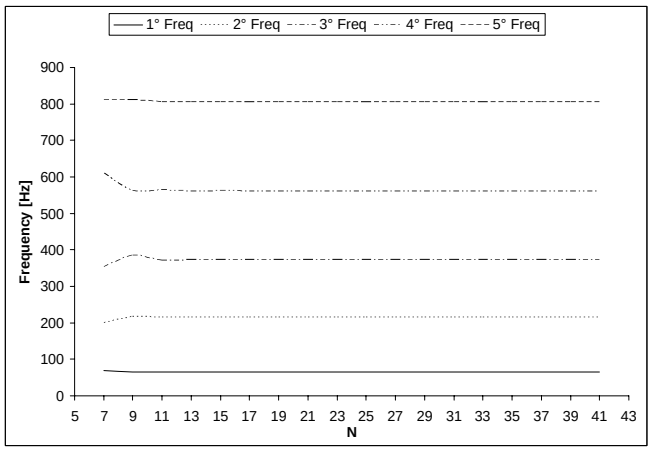

Figure 8 : Convergence characteristics of the first five frequencies for the hinged-hinged tapered arch with centroidal axis radius $r = 1\,m$, width $b = 0.1\,m$, full amplitude $\vartheta_0 = 120^\circ$ and quadratic cross-sectional height variation with $h_0 = 0.08\,m$, $\alpha_0 = 30^\circ$ in damaged configuration. The stiffness of the rotational spring is $K_\varphi = EI$. Angular coordinate of the cracked cross-section: $\vartheta_{cr} = 40^\circ$. The material properties are reported in Table 1.

Figs. 9 and 10 represent the first four modal shapes, for both undamaged and damaged configurations for clamped-clamped and hinged-hinged circular arches, respectively, with quadratic height variation. Furthermore, Fig. 11 shows the 3D modal shapes for the damaged clamped-clamped circular arch with quadratic height variation.

Concerning the undamaged reference configuration, the even and odd modes are, respectively, symmetric and skew-symmetric with respect to the middle section of the arch. The four modal shapes of the hinged arch show a different behaviour, when compared to the others; in fact, the principal displacement component is the radial one, while practically null tangential translation occurs.

In the damaged cases, mode shapes show no symmetry/skew-symmetry anymore and generally differ from the undamaged ones.

7 Conclusion

This paper presents the in-plane free vibrations analysis of circular arches with uniform, continuously varying and stepped cross-sections to illustrate the versatility of the generalized differential quadrature method. Different boundary conditions have been considered. Both undamaged and damaged configurations have been explored, modelling the cracked section as an elastic rotational spring. Examples presented show that the generalized differential quadrature method can produce accurate results utilizing only a small number of sampling points. The G.D.Q. technique provides a very simple algebraic formulation to determine the weighting coefficients required by the differential quadrature approximation without in any way restricting the choice of mesh grids. The discretizing and the programming procedure are easy. Fast convergence and very good stability have been shown. From the numerical computation, it can be concluded that the G.D.Q.E. approach is an efficient method for the vibration analysis of circular arches with varying cross-section in undamaged and damaged configurations due to its high order of accuracy and low requirement for virtual storage and computational effort.

Acknowledgement: This research was supported by the Italian Ministry for University and Scientific, Technological Research MIUR (40% and 60%). The research topic is one of the subjects of the Centre of Study and Research for the Identification of Materials and Structures (CIMEST) - “M. Capurso”.

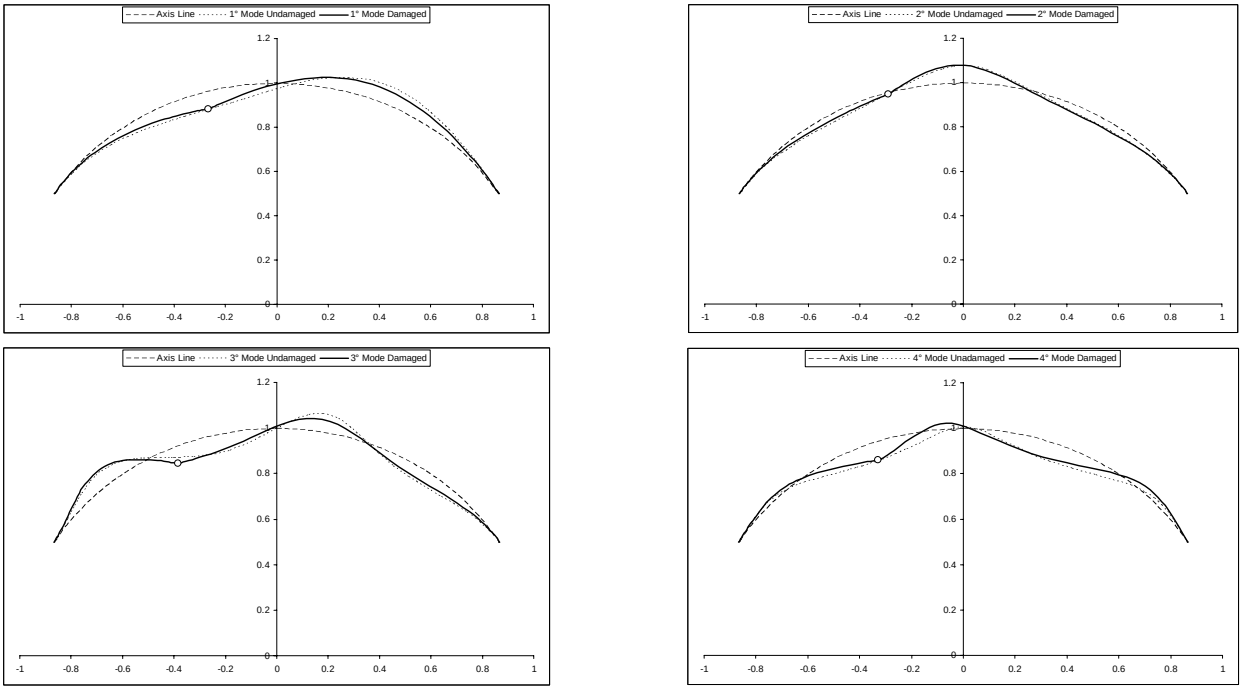

Figure 9 : Modal shapes referring to the free vibrations of the clamped-clamped tapered circular arch with centroidal axis radius $r = 1\,m$, width $b = 0.1\,m$, full amplitude $\vartheta_0 = 120^\circ$ and quadratic cross-sectional height variation with $h_0 = 0.08\,m$ in undamaged and damaged configurations. The stiffness of the rotational spring is $K_\varphi = EI$. Angular coordinate of the cracked cross-section: $\vartheta_{cr} = 80^\circ$. The material properties are reported in Table 1.

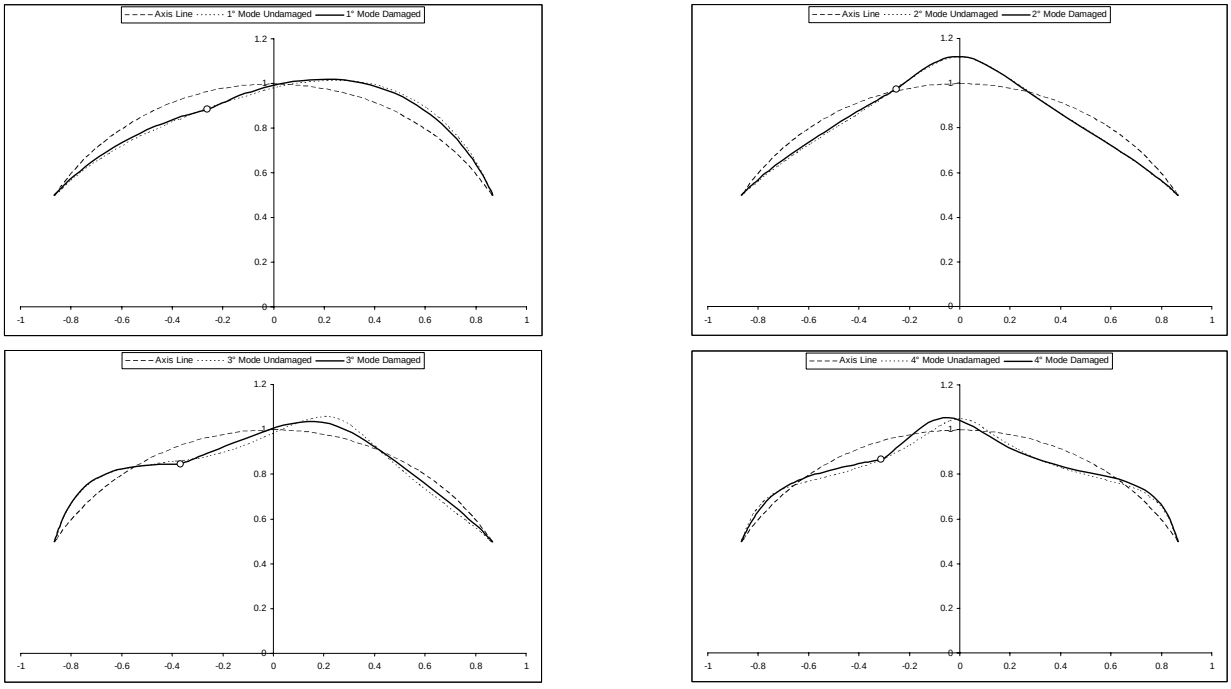

Figure 10 : Modal shapes relative to the free vibrations of the hinged-hinged tapered circular arch with centroidal axis radius $r = 1\,m$, width $b = 0.1\,m$, full amplitude $\vartheta_0 = 120^\circ$ and quadratic cross-sectional height variation with $h_0 = 0.08\,m$ in undamaged and damaged configurations. The stiffness of the rotational spring is $K_\varphi = EI$. Angular coordinate of the cracked cross-section: $\vartheta_{cr} = 80^\circ$. The material properties are reported in Table 1.

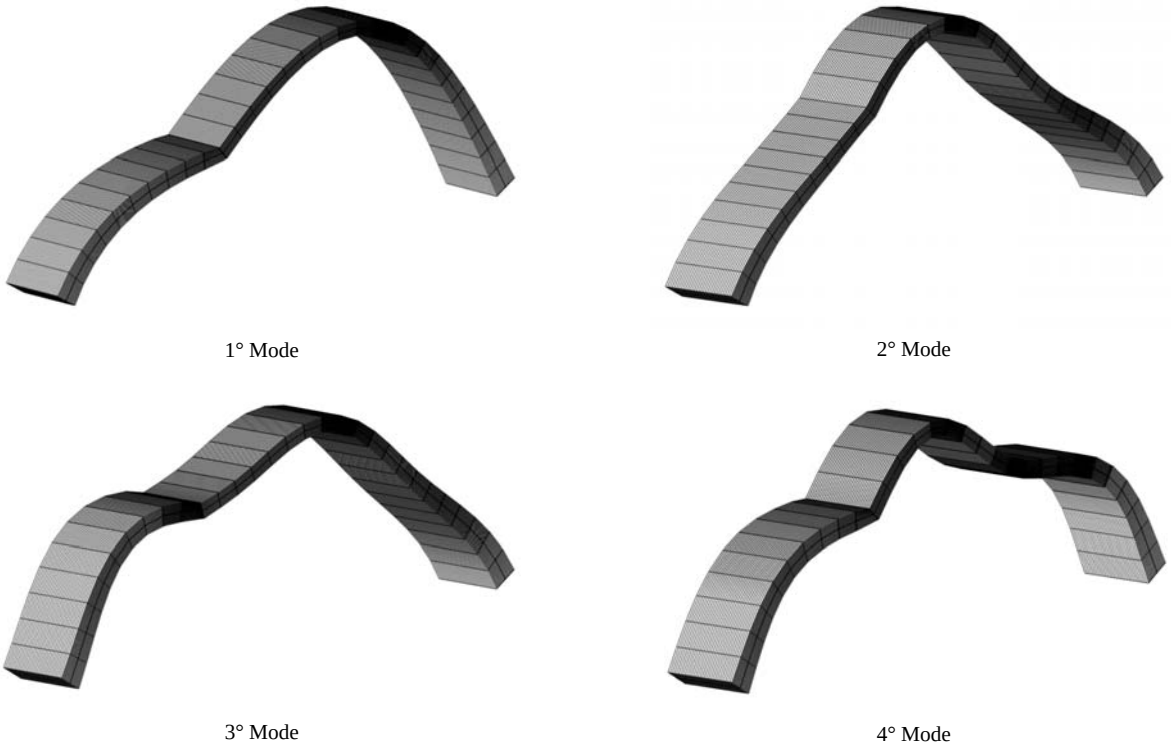

Figure 11 : 3D modal shapes relative to the free vibrations of the clamped-clamped tapered circular arch with centroidal axis radius $r = 1\,m$, width $b = 0.1\,m$, full amplitude $\vartheta_0 = 120^\circ$ and quadratic cross-sectional height variation with $h_0 = 0.08\,m$ in damaged configurations. The stiffness of the rotational spring is $K_\varphi = EI$. Angular coordinate of the cracked cross-section: $\vartheta_{cr} = 80^\circ$. The material properties are reported in Table 1.

References

Bellman, R.; Casti, J. (1971): Differential quadrature and long-term integration. *J Math Anal Appl*, vol. 34, pp. 235-238.

Bellman, R.; Kashef, B. G.; Casti, J. (1972): Differential quadrature: a technique for the rapid solution of nonlinear partial differential equations. *J Comput Phys*, vol. 10, pp. 40-52.

Benedetti, A.; Deseri, L.; Tralli, A. (1996): Simple and effective equilibrium models for vibration analysis of curved rods. *J Eng Mech-ASCE*, vol. 122, pp. 291-299.

Bert, C.; Malik, M. (1996): Differential quadrature method in computational mechanics: a review. *Appl Mech Reviews*, vol. 49, pp. 1-27.

Bert, C. W.; Jang, S. K.; Striz, A. G. (1988): Two new approximate methods for analyzing free vibration of structural components. *AIAA J*, vol. 26, pp. 612-618.

Chen, C.N. (2000): A generalized differential quadrature element method. *Comput Method Appl Mech Eng*, vol. 188, pp. 553-566.

Chondras, T. G.; Dimarogonas, A. D. (1980): Identification of cracks in welded joints of complex structures. *J Sound Vib*, vol. 69, pp. 531-538.

Civan, F.; Sliepcevich, C. M. (1984): Differential quadrature for multi-dimensional problems. *J Math Anal Appl*, vol. 101, pp. 423-443.

Civan, F.; Sliepcevich, C. M. (1985): Application of differential quadrature in solution of pool boiling in cavities. *Proceeding of Oklaoma Academy of Sciences*, vol. 65, pp. 73-78.

De Rosa, M. A.; Franciosi, C. (2000): Exact and approximate dynamic analysis of circular arches using DQM. *Int J Solid Struct*, vol. 37, pp. 1103-1117.

Friedman Z.; Kosmatka, J. B. (1998): An accurate two-node finite element for shear deformable curved beams. *Int J Numer Meth Eng*, vol. 41, 473-498.

Gutierrez, R. H.; Laura, P. A. A. (1995): Vibrations of non-uniform rings studied by means of the differential quadrature method. *J Sound Vib*, vol. 185, pp. 507-513.

Kang, K.; Bert, C.W.; Striz, A.G. (1995): Vibration analysis of shear deformable circular arches by the differential quadrature method. *J Sound Vib*, vol. 181, pp. 353-360.

Kang, K.; Bert, C.W.; Striz, A.G. (1996): Vibration and buckling analysis of circular arches using DQM. *Comput Struct*, vol. 60, pp. 49-57.

Karami, G.; Malekzadeh, P. (2003): Application of a new differential quadrature methodology for free vibration analysis of plates. *Int J Numer Meth Eng*, vol. 56, pp. 847-868.

Karami, G.; Malekzadeh, P. (2004): In-plane free vibration analysis of circular arches with varying cross-sections using differential quadrature method. *J Sound Vib*, vol. 274, pp. 777-799.

Liu, G. R.; Wu, T. Y. (2001): In-plane vibration analyses of circular arches by the generalized differential quadrature rule. *Int J Mech Sci*, vol. 43, 2597-2611.

Quan, J. R.; Chang, C. T. (1989): New insights in solving distributed system equations by the quadrature method – I. Analysis. *Comput Chem Eng*, vol. 13, pp. 779-788.

Rizos, P. F.; Aspragathos, N. T.; Dimarogonas, A. D. (1990): Identification of crack location and magnitude in a cantilever beam from the vibration modes. *J Sound Vib*, vol. 138, pp. 381-388.

Shu, C. (1991): Generalized differential-integral quadrature and application to the simulation of incompressible viscous flows including parallel computation. *PhD Thesis*, University of Glasgow.

Shu, C. (2000): Differential Quadrature and its Application in Engineering. Springer: Berlin.

Shu, C.; Chen, W. (1999): On optimal selection of interior points for applying discretized boundary conditions in DQ vibration analysis of beams and plates. *J Sound Vib*, vol. 222, pp. 239-257.

Shu, C.; Chen, W.; Hue, H.; Du, H. (2001): Numerical study of grid distribution effect on accuracy of DQ analysis of beams and plates by error estimation of derivative approximation. *Int J Numer Meth Eng*, vol. 51, pp. 159-179.

Shu, C.; Richards, B. E. (1992): Application of generalized differential quadrature to solve two-dimensional incompressible Navier-Stokes equations, *Int J Numer Meth Fl*, vol. 15, pp. 791-798.

Tong, X.; Mrad, N.; Tabarrok, B. (1988): In-plane vibrations of circular arches with variable cross-sections. *J Sound Vib*, vol. 212, pp. 121-140.

Tornabene, F.; Viola, E. (2005): The effect of cracks on the dynamic response of circular arches with varying cross-section by G.D.Q.E. Technique. In: M. H. Aliabadi et al. (eds), *Advances in Fracture and Mechanics IV*, EC, Ltd, Eastleigh, England, pp. 295-300.

Tüfekçi, E.; Arpaci, A. (1998): Exact solution of in–plane vibrations of circular arches with account taken of axial extension, transverse shear and rotatory inertia. *J Sound Vib*, vol. 209, pp. 845-856.

Viola, E.; Federici, L.; Nobile, L. (2001): Detection of crack location using cracked beam element method for structural analysis. *Theor Appl Fract Mech*, vol. 36, pp. 23-35.

Viola, E.; Nobile, L.; Federici, L.; (2002): Formulation of crack beam element method for structural analysis. *J Eng Mech-ASCE*, vol. 128, pp. 220-230.